Journal of Power Sources 571 (2023) 233016

Contents lists available at ScienceDirect

Journal of Power Sources

journal homepage: www.elsevier.com/locate/jpowsour

Development of a high-energy electrical double-layer capacitor demonstrator with 5000 F in an industrial cell format

Lukas Köps [a], Peter Ruschhaupt [b,c], Chris Guhrenz [d], Philipp Schlee [d], Sebastian Pohlmann [d], Alberto Varzi [b,c], Stefano Passerini [b,c], Andrea Balducci [a,*]

[a] Friedrich-Schiller-University Jena, Institute for Technical Chemistry and Environmental Chemistry and Center for Energy and Environmental Chemistry Jena (CEEC Jena), Philosophenweg 7a, 07743, Jena, Germany
[b] Helmholtz Institute Ulm (HIU), Helmholtzstrasse 11, D-89081, Ulm, Germany
[c] Karlsruhe Institute of Technology (KIT), P.O. Box 3640, D-76021, Karlsruhe, Germany
[d] Skeleton Technologies GmbH, Schücostraße 8, 01900, Großröhrsdorf, Germany

HIGHLIGHTS

- Introducing novel materials into industrial demonstrators.
- Demonstrator with nominal capacitance of 5000 F and energy density of 12.2 Wh L^{-1}.
- Capacitance retention of 77% after 1400 h of float at 2.85 V and 65 °C.

ARTICLE INFO

Keywords:
Demonstrator
High energy
High capacitance
Industrial
Prototype
Supercapacitor

ABSTRACT

The introduction of novel materials into industrial demonstrators is an essential step in developing unique commercial energy storage devices. However, this step is rarely considered in literature. In this study, we report on the introduction of innovative materials for high energy density electrical double-layer capacitors (EDLCs), namely the carbide-derived carbon (CDC) "Curved Graphene" with a specific and an aerial capacitance of 114 F g^{-1} and 82 F cm^{-3}, polysaccharide binders, and electrolyte based on acetonitrile (ACN) and pyrrolidinium-based salt, into a demonstrator. We show that by utilizing this innovative cell chemistry it is possible to realize an industrial demonstrator exhibiting a nominal capacitance of 5000 F, with a specific energy and energy density of up to 8.4 Wh kg^{-1} and 12.2 Wh L^{-1} as well as a remarkable lifetime with a capacitance retention of 77% after floating for almost 1400 h at 2.85 V and 65 °C. These results prove that the novel materials considered in this work can indeed be utilized for the realization of commercially available devices with improved cell performance with respect to the state-of-the-art.

1. Introduction

Digitalization and the connected demand for electrical energy in stationary and mobile applications require smart solutions in the field of electrical energy storage. Among modern energy storage technologies, lithium-ion batteries (LIBs) are most widely spread due to their high energy density as well as their relatively high stability and lifetime [1]. However, the power density of LIBs is limited and for some applications not sufficient while their safety is still a major concern. As an alternative energy storage technology, supercapacitors or ultracapacitors offer a superior power density with an extremely long lifetime [2–4].

The most popular and only commercially available types of supercapacitors are the electrical double-layer capacitors (EDLCs) [5]. These devices are relying on a physical charge storage process, in which the ions of the electrolyte form a capacitive double-layer on the surface of the electrodes upon the application of a voltage to the device. This process is extremely efficient, enabling an outstanding lifetime – in the order of several million cycles – and especially outstanding when considering short power pulses in which batteries are limited by reaction kinetics enabling the possibility to charge these devices in very short time frames [6–8]. The major drawback of EDLCs is their limited energy density (~ 5–8 Wh kg^{-1}) which is preventing their use in applications

* Corresponding author.
E-mail address: andrea.balducci@uni-jena.de (A. Balducci).

https://doi.org/10.1016/j.jpowsour.2023.233016
Received 3 November 2022; Received in revised form 16 March 2023; Accepted 27 March 2023

where also a relatively high amount of energy is required [9–14]. Generally, the energy density of EDLCs depends on the capacitance (C) of the electrode material and the operative voltage (V) of the device, which is determined by the used electrolyte ($E = 1/2CV^2$) [15–17]. Therefore, in recent years, research focused on increasing the capacitance as well as the operative voltage by developing novel electrode and electrolyte materials.

State-of-the-art EDLCs consist of composite electrodes containing classically activated carbon (AC) with a relatively broad pore size distribution as active material, carbon black as conductive additive, and a binder, such as sodium carboxymethyl cellulose (NaCMC) [18,19]. As the electrolyte, solutions containing tertiary ammonium salts, e.g., ammonium tetrafluoroborate, dissolved in acetonitrile (ACN) or propylene carbonate (PC) are used [20,21]. This electrode-electrolyte combination allows the realization of devices with maximum operating voltages in a range between 2.7 and 3.0 V.

In the last 10 years, a large number of alternative electrode and electrolyte components have been proposed [21–28]. Although yielding promising results on material-level performance, these alternative materials have been mainly tested in lab scale cells. For this reason, it is often not clear how their properties are translating into "real" devices. This is, of course, a limitation, while considering the realization of innovative EDLCs with superior performance with respect to state-of-the-art devices [29].

With the aim to supply information on the impact of novel materials on EDLCs performance, in this work, we are reporting about the realization and testing of an industrial EDLC demonstrator with a capacitance of 5000 F containing innovative electrode and electrolyte components. These developments pave the way for a breakthrough in energy density.

2. Material and methods

2.1. Active material investigations

The elemental composition (C, H, and N) was determined with the Elemental Analyzer vario MACRO cube according to the International Standard EVS-ISO 29541:2015 while the oxygen content was determined with the Elemental Analyzer ECS4010 based on the Elementar Rapid OXY cube instruction. For this purpose, a sample of 5–10 mg was heated to 1400 °C in a helium atmosphere to convert the oxygen in the sample to CO, which was then detected quantitatively by an infrared detector.

The pore size distributions of the carbon materials were determined by N_2 sorption measurements at 77 K using a 3 Flex gas sorption analyzer (Micromeritics). The samples were degassed at 350 °C under vacuum for 12 h before analysis. The pore size distributions were calculated by Non-Localized Density Functional Theory (NLDFT) at 77 K on slit pore models.

2.2. Binder investigations

Potato starch (PS) was purchased from Sigma Aldrich. CMC was purchased from Dow Wolff Cellulosics (CMC Walocell 2000 PA). Activated carbon (AC, namely YP50 from Kuraray), rubberizing agent (RA), and etched aluminum foil (20 μm, 5.18 mg cm^{-2}) were kindly supplied by Skeleton Technologies GmbH. Carbon black (CB) was purchased from Imerys Graphite & Carbon (C-ENERGY Super C45). All slurries were prepared with weight ratios of AC: CB: binder of 93 : 2.8: 4.2. A commercial rubberizing additive (RA) was included in the various investigated binders in the amount of 2.33 wt% (included in the binder weight). This means that, in case of a single binder such as CMC100, the binder was indeed 1.87 wt% CMC and 2.33 wt% RA. In case of a double binder mixture such as XG50/CMC50, the binder composition was: 0.94 wt% XG, 0.94 wt% CMC and 2.33 wt% RA. The solid content of the slurries was adjusted to achieve homogenous coatings, but as close as possible to 33% as required for industrial scale-up. The binder was stirred in ultrapure water (milli Q) until fully dispersed. CB, AC, and RA were added successively while mixing with an overhead lab mixer until homogenous.

The slurries were coated onto Al foils with a doctor blade at 50 mm s^{-1} at 250–350 μm wet coating thickness. Coatings were allowed to dry at room temperature for about 30 min and then dried overnight at 80 °C. Bending tests were done with 2.5 cm wide strips cut from dried and calendered electrodes on 6 mm diameter steel rods.

For the electrolyte preparation in the binder-related investigations, tetraethylammonium tetrafluoroborate ($TEABF_4$), and acetonitrile (ACN) were purchased from Sigma Aldrich. Electrodes were cut into 12 mm disks and dried at 110 °C in vacuum overnight and transferred to an argon-filled glove box (LabMaster, Mbraun GmbH) with <0.1 ppm O_2 and <0.1 ppm H_2O for cell assembly. Stainless steel Swagelok-type three-electrode cells were used for voltage hold and EIS experiments using Mylar foil as insulator between the cell parts and the outer casing. About 150 μL of electrolyte were impregnated into glass fiber disks (GF/D, thickness: 670 μm, diameter: 13 mm diameter; Whatman). EIS experiments were performed on symmetric cells with 9 mg cm^{-2} mass loadings using an Impedance/Gain-Phase Analyzer 1260 (Solartron Analytical). EIS fits were computed with ZView 2 (Scribner Associates). For voltage hold experiments, two-electrode balanced EDLCs were assembled employing electrodes with a mass loading ranging from ca. 4.1 mg cm^{-2} to 10.0 mg cm^{-2} and a m_{pos}/m_{tot} ratio of 0.7. In such tests, electrodes compressed by a factor of 0.4 were used (limited by the maximum possible compression of CMC electrodes). Furthermore, the overall mass of the CMC-based electrodes was reduced but kept at the same m_{pos}/m_{tot} ratio of 0.7. This was done because high-loading CMC-based electrodes form cracks and could not be otherwise tested. The cells were cycled using a battery tester (Maccor 4300), using a protocol of 25 h voltage hold steps with five short evaluation cycles in between the steps to determine the capacitance by integration [19]. All electrochemical tests were performed in climatic chambers at T = 20 °C ± 2 °C (KB115, Binder GmbH).

2.3. Electrolyte investigations

The investigated solvent ACN was purchased from Sigma Aldrich with a purity of 99.8% and dried over molecular sieve with a pore size of 3 Å until the water content was reduced to <20 ppm. The electrolyte salts, namely $TEABF_4$, *N,N*-butylmethylpyrrolidinium tetrafluoroborate ($Pyr_{14}BF_4$), and *N,N*-dimethylpyrrolidinium tetrafluoroborate ($Pyr_{11}BF_4$) were provided by IoLiTec (Germany) and additionally dried before use in a vacuum glass oven at 120 °C and 1×10^{-2} mbar for 24 h to reduce the initial water content to <20 ppm. The electrolyte solution and electrochemical cells were prepared in an argon-filled Labmaster pro glove box from MBRAUN with H_2O and O_2 contents of the argon atmosphere <1 ppm. For assembling the cells, stainless steel Swagelok-type cells were used in a two-electrode setup with industrial composite electrodes with a mass loading of 68 g m^{-2} provided by Skeleton Technologies GmbH. In order to match the experimental setup, one side of the double-sided AC coating was removed. Afterward, circular disks with an area of 1.13 cm^2 were punched out. The symmetrical electrodes were separated by a 520 μm Whatman glass fiber disk which was soaked with 120 μL of the investigated electrolyte solutions.

Ionic conductivity measurements were performed with a Solartron Modulab XM ECS, while the conductivity cell was placed in a climatic chamber to adjust the temperature between -30 and 80 °C. The measurements were carried out identically to reference [30]. Viscosity measurements were conducted with an Anton-Paar MCR 102 rotational viscometer and 500 μL of the electrolyte solution in a temperature range between -30 – 50 °C at a shear rate of 1000 s^{-1} as described in reference [30].

To investigate the stability of the electrolytes, the electrochemical

measurements were carried out using an Arbin LBT21084 potentiostat/galvanostat by applying constant voltage for 20 h and five galvanostatic charge-discharge cycles with a current rate of 1 A g^{-1} in between to determine the capacitance retention.

2.4. Demonstrator assembly

The electrode paste, the so-called slurry, for the preparation of the electrode for the industrial 5000 F EDLC was produced according to Skeleton's standard recipe applying "Curved Graphene" as the active material. After coating the etched aluminum foil, the resulting double-side coated electrode was calendered and slit according to the required specifications for the cell assembly. The following assembly process steps were performed according to industrial standards and were similar to Skeleton's standard product series of the classical SCA3200 cell [31]. The training program of the demonstrator consisted of two galvanostatic cycles at 10 A between 0 and 2 V and 15 min voltage hold at 2 V followed by two cycles at 10 A between 1 and 2.5 V and a subsequent voltage hold for 15 min at 2.5 V. After discharging the demonstrator to 0 V, it was charged to 2.7 V and further to 2.85 V with 5 min of voltage hold at both indicated voltages before it was discharged to 0 V and cooled down. The stability of the demonstrator was investigated by floating tests for 1500 h where five galvanostatic cycles with 50 A were performed in between the voltage holding phases to determine values for capacitance and ESR.

3. Results & discussion

3.1. Active material and electrode

The current state-of-the-art technology for EDLCs uses activated carbon (AC) as the electrode material, in most cases derived from the pyrolysis of coconut shells [32,33]. Skeleton's patented "Curved Graphene" Technology represents a significant leap toward an affordable, proven, and scalable increase in energy for high-power energy storage devices while keeping the power in those devices at a similar level as before. "Curved Graphene" provides the possibility to tailor the ratio of micro-to mesopores to the respective application needs. As the capacitive energy storage process in EDLCs is localized predominantly in micropores (d < 2 nm), a large amount of micropore volume is required. Optimized ACs generally provide a micropore ratio of 0.5–0.6 [34–37]. Higher values cannot be reached due to the amorphous structure of the respective precursor materials, such as coconut shells, which gives rise to highly disordered carbon structures. The porosity of carbon materials is a result of the interplay of the precursor chemistry and the process parameters in the thermal conversion process of the precursor material to the final carbon material. The porosity of ACs derived from amorphous organic precursors can only be optimized by changing process parameters empirically as the structure of the precursor is mainly amorphous. Therefore, Skeleton Technologies has chosen a fundamentally different approach: Starting from a crystalline precursor with a known structure and conversion of the crystalline precursor by a known reaction mechanism. Due to these changes, a completely novel class of active carbon, namely "Curved Graphene", can be produced in a highly controlled manner. "Curved Graphene" can provide a micropore ratio of up to 0.95, maximizing capacitive energy storage as can be seen in Fig. 1a. The local structural information is further depicted in scanning electron microscopy (SEM) and transmission electron microscopy (TEM) images in the Supplementary Information (Fig. S1 & Fig. S2). In order to increase the operating voltage of an energy storage device, the application of novel electrolyte solvents, conductive salts, and additives is needed [38,39]. In conclusion, this results in new demands for the optimization of pore sizes within the active material. Thus far, only "Curved Graphene" offers the possibility to tune the majority of the pores to fit within a narrow size band.

Due to the known precursor structure and the high control over the chemistry and process parameters, "Curved Graphene" exhibits a significantly higher purity than ACs derived from organic precursors (Fig. 1b and Table 1) which in turn leads to fewer side reactions and increases the lifetime of the cell, especially at higher operating voltages and temperatures.

The electrode was coated according to Skeleton's standard (aqueous) slurry recipe applying "Curved Graphene" as the activated carbon together with a conductive additive and binders for flexibility of the electrode and adhesion of the particles between each other and towards the foil. The resulting double-side coated electrode was calendered to reach both lower equivalent series resistance (ESR) and higher capacitance in the final demonstrator cell. Due to the significantly increased electrode density, a much larger amount of active material could be accommodated in Skeleton's standard SCA3200 cell. Both the highly porous structure and the higher carbon content/cell resulted in the fabrication of a 5000 F cell applying the same D60 standard form factor, which today yields between 3000 and 3400 F [29]. This is an overall energy density increase of 56%.

3.2. Binder investigations

Carboxymethyl cellulose (CMC) is the current industry standard

Table 1
Elemental composition of commercial activated carbon and "Curved Graphene". The given elemental fractions are related to their mass.

Carbon Type	Carbon	Nitrogen	Hydrogen	Oxygen
Activated carbon, commercial	95%	0.6%	0.2%	4.2%
Curved Graphene	98.5%	0.5%	0.2%	0.8%

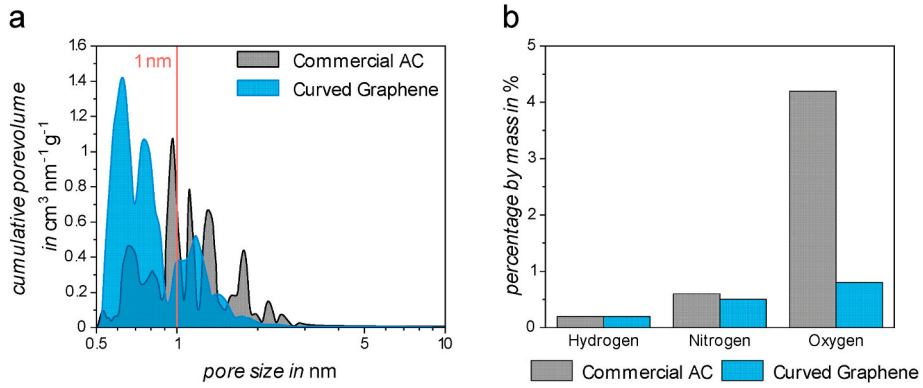

Fig. 1. a) Cumulative pore volume of "Curved Graphene" compared to commercial activated carbon (AC), b) content of heteroatoms in "Curved Graphene" compared to commercial AC.

binder. However, even when a rubberizing agent (RA) is added to the slurry, like styrene-butadiene rubber (SBR), CMC tends to crack upon drying due to shrinkage of the coating if the mass loadings are too high [40]. Several other natural polymers (potato starch, wheat starch, guar gum) proved impressive flexibility at high loading, even without the addition of a RA. However, electrodes based on such polysaccharides are difficult to densify, as they easily delaminate upon calendering [19]. Presumably, this is due to the lower cohesion between the coating particles, which on one hand prevents cracking, but on the other hand, causes disintegration of the coating when exposed to the high shear stresses of calendering. This compression step is however crucial to maximize the energy density (Wh cm^{-3}), which for most applications is more relevant than the specific energy (Wh kg^{-1}). In fact, non-calendered electrodes typically have 20% lower density than calendered ones. Additionally, calendering helps to improve the handling of the electrode rolls in an industrial setup since the electrode surface becomes much more abrasion-resistant.

To improve the mechanical properties of the electrode without penalizing the electrochemical response, mixtures of polysaccharides (potato starch (PS), xanthan gum (XG)) and CMC (with a RA) are developed to both reduce the shrinking and cracking issues typical of CMC, yet allowing for densification by calendering. Binders formulations are dubbed by their content of binder, e.g., PS50/CMC50 for a 1:1 wt ratio of PS and CMC, or CMC100 for electrodes with CMC as the only binder (besides the RA).

Calendering was done with successively higher compression up to a minimum slit width of 30% of the original electrode thickness (0.3 compression). Fig. 2a shows the resulting thicknesses and densities achieved. As shown in the right-hand photograph, the standard formulation CMC100 could not be compressed to more than 0.61 g cm^{-3} (compression rate 0.4) without delaminating (denoted by the empty circle in the compression plot). PS50/CMC50 could also not be compressed beyond this density, but no delamination occurred upon higher compression (see Fig. 2b). So, these two binder formulations can be

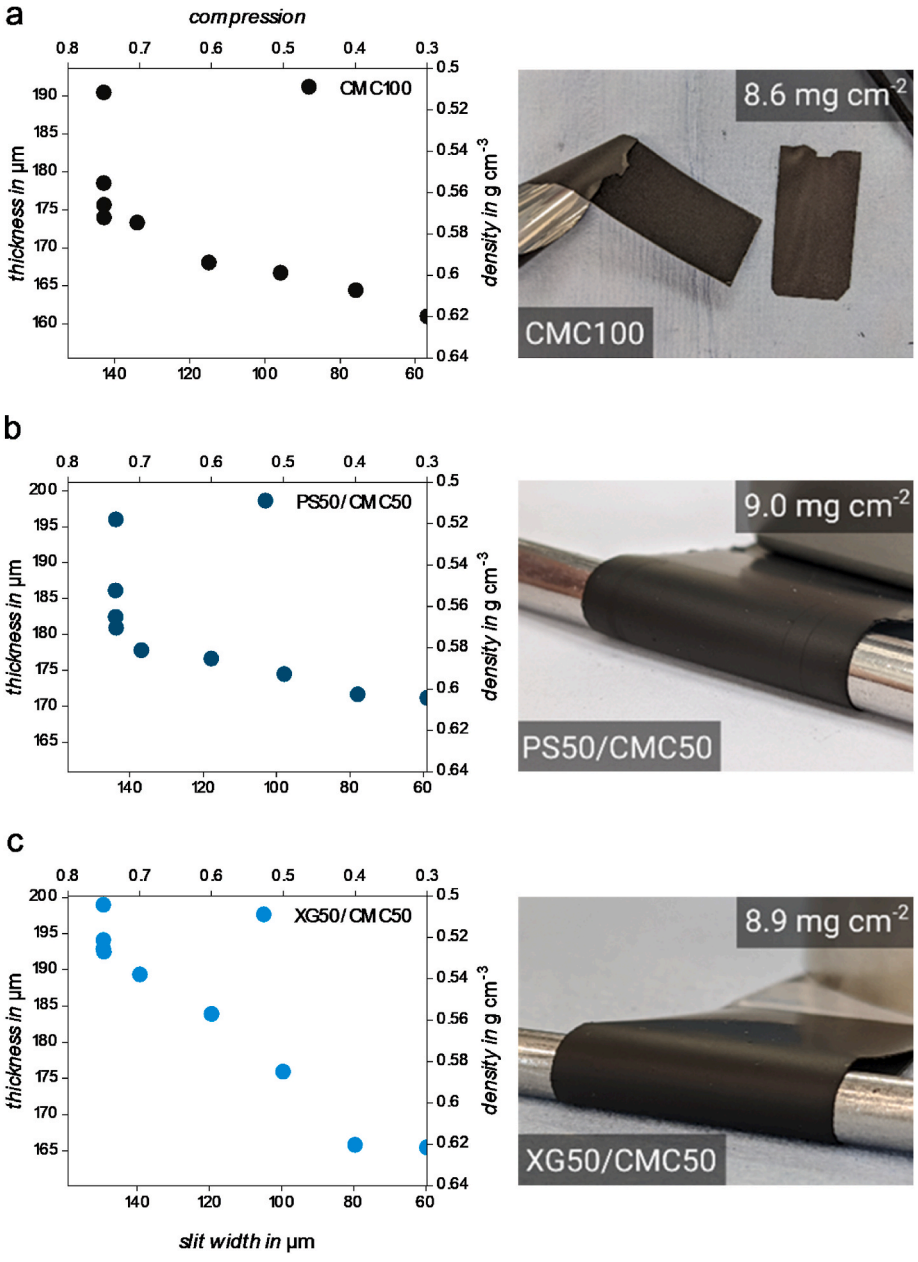

Fig. 2. Effect of calendering on electrode densification and successive bending tests on a 6 mm rod with a) CMC100, b) PS50/CMC50, and c) XG50/CMC50 as binder formulations.

considered comparable. As opposed to this, higher-density electrodes could be achieved with the XG50/CMC50 mixture, yielding a density of 0.62 g cm^{-2} (see Fig. 2c). Also, both mixed binder formulations demonstrated improved flexibility compared to CMC100 during the 6 mm radius bending test without delaminating and reached a higher areal loading of ca 9 mg cm^{-2}. Consequently, in terms of the properties of the obtained coating, the XG50/CMC50 can be considered the best binder combination among all other investigated materials, including the industrial standard CMC100 [19].

As previously mentioned, binders do not only determine the mechanical properties of EDLC electrodes but also their microscopic morphology, i.e., the distribution of conductive additive between the active material particles. This influences the electrode resistance, which is affected by particle-particle as well as particle-current collector contact resistances [41]. Both can be strongly reduced by calendering which, in turn, is influenced by the binder again, as shown above. Therefore, to elucidate the effect of the binder mixtures on the resistance of the electrodes after calendering, EIS was employed. In order to avoid artifacts, symmetric cells were used [42].

Fig. 3 shows the Nyquist plots resulting from the EIS analysis, including the experimental and simulated spectra (Fig. 3a), and the two equivalent circuits used for the fitting (Fig. 3b and c). All spectra display one or more semicircles at high frequencies. According to previous studies, these can arise from poor contact at the particle-particle and/or particle-current collector interfaces, with the semicircle at higher frequencies generally attributed to the current collector interface [19]. In the case of CMC100 and XG50/CMC50, the spectra can be modeled with an equivalent circuit consisting of a resistor R_{el} for the electrolyte (and an inductance in series due to the cell connections, not shown for simplicity), an R|CPE element with a resistance R_{tot} and a constant phase element CPE_{tot} connected in parallel for the particle-particle interface. A finite-space Warburg, commonly known as "open" Warburg (W_o) is used to model the low-frequency part of the spectra. This element is particularly suitable to model a capacitor electrode, since it tends towards a capacitive-like behavior due to the blocking character of the porous carbon (see the equivalent circuit in Fig. 3b). For PS50/CMC50 another R|CPE element had to be included to account for the additional semicircle centered at 222 kHz, as clearly the two different interfaces can be resolved (probably particle-current collector, $R_{cc}|CPE_{cc}$; and particle-particle, $R_{pp}|CPE_{pp}$) (see Fig. 3c). The resistance values obtained from the fits (see Table 2) indicate that PS50/CMC50 significantly increases the current collector interface resistance. In fact, R_{cc} for PS50/CMC50 is larger than the combined interface resistances for particles and current collector (i.e., R_{tot}) of CMC100 and XG50/CMC50. For PS50/CMC50 the values are $R_{cc} = 0.56\ \Omega$ vs. $R_{tot} = 0.55\ \Omega$ and $0.39\ \Omega$ for CMC100 and XG50/CMC50, respectively. Contrarily, in CMC100 and XG50/CMC50 the resistance at the current collector interface is clearly too small to be individually resolved and the frequency of the semicircle indicates most of the resistance results from the particle-particle interfaces. XG50/CMC50 exhibits even lower overall resistance (−29%) than the standard CMC100. This is most likely a direct result of the higher density attainable with XG50/CMC50. XG50/CMC50 must also have lower particle-particle resistance R_{pp} than PS50/CMC50, as the overall resistance value R_{tot} is lower than the lower frequency component of PS50/CMC50 ($R_{tot} = 0.39\ \Omega$ vs. $R_{pp} = 0.40\ \Omega$).

Table 2
Comparison of resistance values obtained from EIS spectra fits for different binder formulations.

Resistance Type	CMC100	PS50/CMC50	XG50/CMC50
R_{pp}	≅ 0.55 Ω	0.4 Ω	≅ 0.39 Ω
R_{cc}	–	0.56 Ω	–
R_{tot}	0.55 Ω	0.96 Ω	0.39 Ω

Lastly, in order to exclude issues of electrochemical degradation that may lead to loss of integrity of the electrode, long-term float voltage tests were performed. Electrodes were taken from electrode sheets which were calendered up to 0.4 compression, which all samples allowed for (see previously discussed calendering tests). The corresponding densities were therefore 0.61 g cm^{-3} (CMC100), 0.61 g cm^{-3} (PS50/CMC50), and 0.62 g cm^{-3} (XG50/CMC50). To achieve results as representative for industrial application as possible, balanced cells were employed, with a mass ratio $m_{positive}/m_{total}$ of 0.7, based on stability potential limits of +0.9 V and −1.9 V vs. AC immersion potential [43–45]. These cells were subjected to repeated 25 h voltage hold periods at 2.8 V cell voltage with short periods of slow cycling in between to measure the capacitance retention [19]. As shown in Fig. 4, the performance of both selected binder mixtures is virtually identical to that of CMC100. The specific capacitance was around 22 F g^{-1}. All cells showed comparable performance decay, probably limited by the decomposition of the ACN-based standard electrolyte. This final test, therefore, shows that PS50/CMC50 and XG50/CMC50 can improve the energy density of supercapacitors without any additional downside in

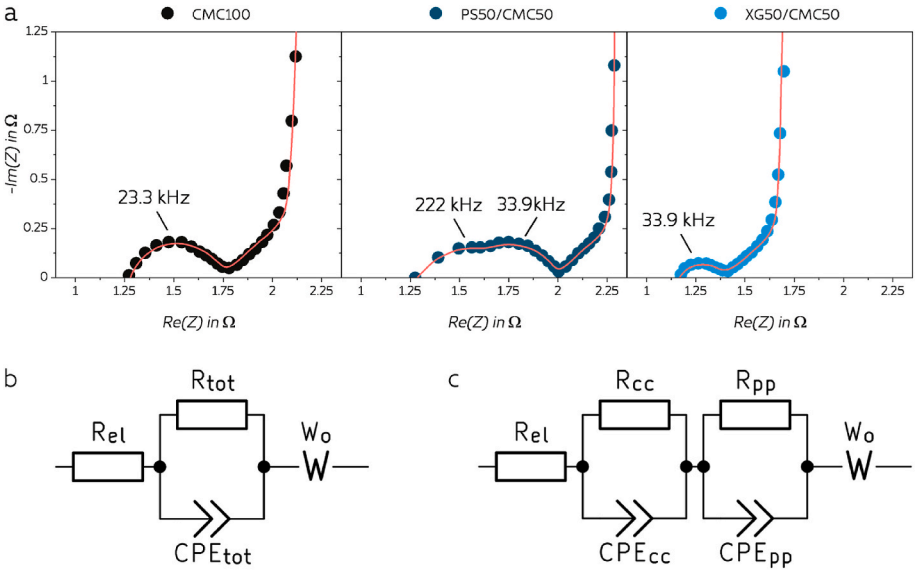

Fig. 3. a) Experimental and simulated EIS spectra of symmetric cells including electrodes with the two most promising binder formulations, and CMC100 as a control sample. b) Equivalent circuit used to fit the spectra of CMC100 and XG50/CMC50 and (c) PS50/CMC50 respectively.

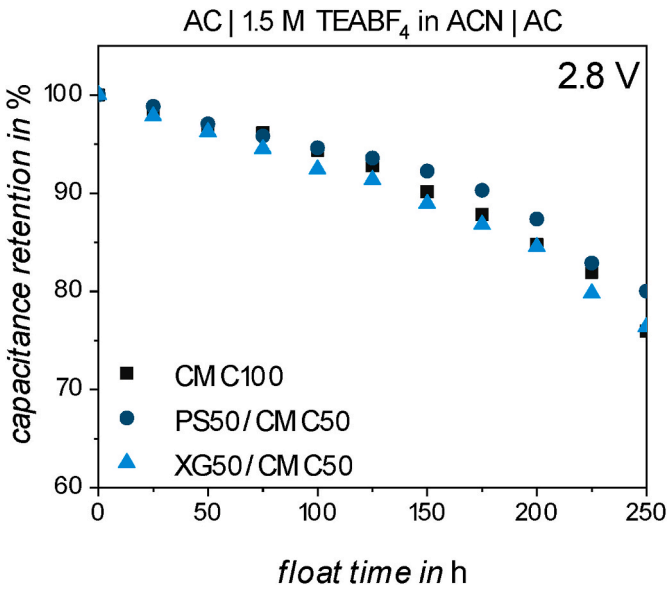

Fig. 4. Capacitance retention of balanced activated carbon (AC) full cells upon voltage hold tests at 2.8 V.

terms of performance and, potentially, at a lower cost.

3.3. Electrolyte investigations

Fig. 5a–b depicts and compares the impact of the temperature on the viscosity and conductivity of the conventional electrolyte 1 M $TEABF_4$ in ACN and on the alternative electrolytes 1 M $Pyr_{14}BF_4$ in ACN and 2 M $Pyr_{11}BF_4$ in ACN. Due to the utilization of ACN as solvent in all investigated electrolytes, the ionic conductivity (Fig. 5a) is generally high compared to carbonate-based electrolytes. However, there is a clear influence of the conductive salt visible. While the state-of-the-art electrolyte based on $TEABF_4$ displays a conductivity of 38.8 mS cm^{-1} at 20 °C, the pyrrolidinium-based electrolytes show higher ionic conductivity at this temperature reaching 42.9 mS cm^{-1} for the $Pyr_{14}BF_4$ based and 56 mS cm^{-1} for the $Pyr_{11}BF_4$ based electrolyte. When increasing the temperature, the conductivity of the reference electrolyte increases more than the conductivity of the $Pyr_{14}BF_4$-based electrolyte. Still, $Pyr_{11}BF_4$ shows the highest conductivity over the whole temperature range which is partially affected by the higher amount of charge carriers due to the higher salt concentration. However, the higher salt concentration means significantly higher cost for an industrial application and therefore does not necessarily justify the increased performance [12]. While the pyrrolidinium-based electrolytes tend to provide higher ionic conductivities than the reference electrolyte, the viscosity depicted in Fig. 5b shows a different trend. With 0.5 mPa s at 20 °C, the state-of-the-art electrolyte displays the lowest viscosity. In contrast to that, the pyrrolidinium-based electrolytes show viscosities of 0.8 mPa s for the $Pyr_{14}BF_4$ based and 0.9 mPa s for the $Pyr_{11}BF_4$-based electrolytes.

With the aim to investigate the impact of these electrolytes on the stability of EDLCs, floating measurements at a constant voltage of 3.0 V at 20 °C were performed with a symmetrical cell setup. This operative voltage was selected as it is achievable by some of the most advanced EDLCS released on the market. Therefore, it can be considered as a representative value to evaluate the potential of the investigated electrolytes in the application of the demonstrator or commercial use. Fig. 5c shows the floating stability of the investigated EDLCs by depicting their capacitance retention over 500 h. Remarkably, all investigated systems display capacitance retentions of >80% – which is commonly defined on lab scale as end-of-life criteria – after 500 h of constant voltage. According to previous studies, 500 h of floating is roughly comparable to 1,500,000 cycles of charge and discharge at 1 A g^{-1}, meaning, that the

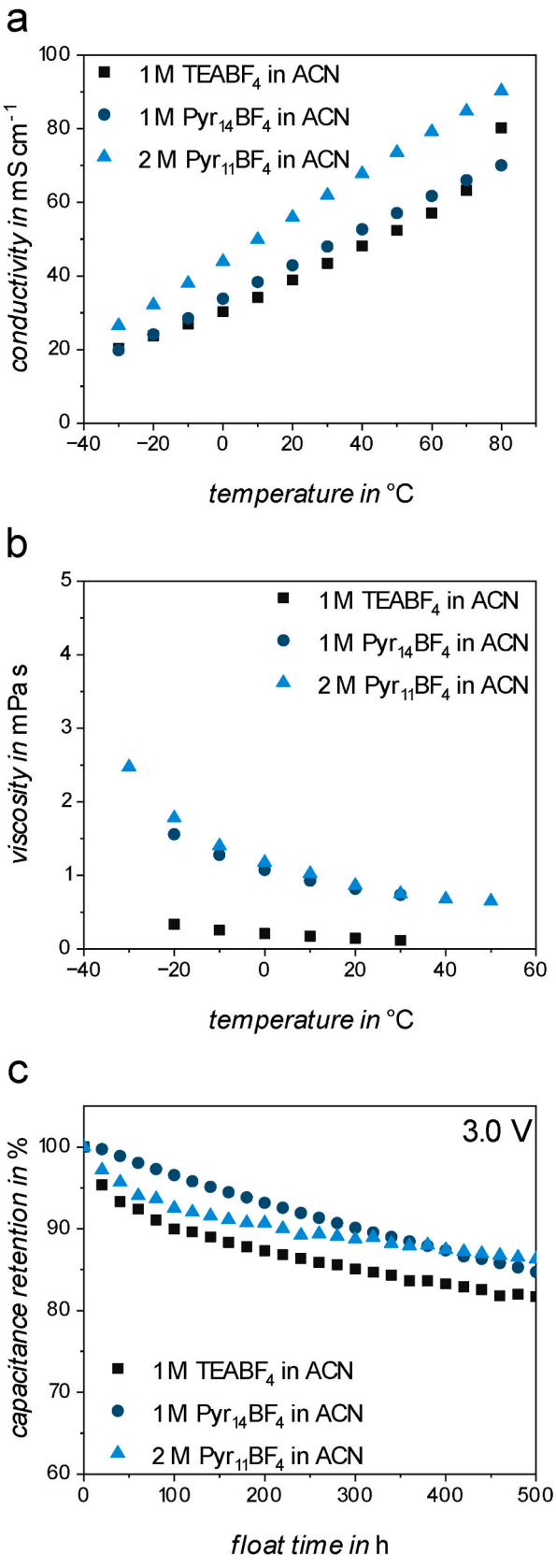

Fig. 5. Comparison of the temperature dependency of a) ionic conductivity and b) viscosity and c) comparison of the floating stability at 3.0 V and 20 °C of 1 M $TEABF_4$ in ACN, 1 M $Pyr_{14}BF_4$ in ACN, and 2 M $Pyr_{11}BF_4$ in ACN.

use of these electrolytes allows for several million charge-discharge cycles [46]. Among these electrolytes, 2 M $Pyr_{11}BF_4$ in ACN displays remarkable stability with a capacitance retention of 86% while the $TEABF_4$ and $Pyr_{14}BF_4$-based electrolytes show lower stability and a capacitance retention of 82% and 85%, respectively. These results highlight the promising properties of pyrrolidinium salts which can provide higher electrochemical stability than the conventional tetraalkylammonium salts and are, therefore, suitable to exploit in commercial applications. However, it has to be kept in mind that industrial lifetime testing is conducted at 65 °C which will shorten the lifetime compared to 20 °C measurements significantly.

3.4. Electrode preparation and demonstrator assembly

The general demonstrator assembly process is divided into three steps: 1.) electrode production, including slurry mixing, double-side electrode coating, calendering, and slitting; 2.) jelly-roll winding and cell assembly (incl. Electrolyte filling), and 3.) cell testing.

The aqueous slurry was produced according to Skeleton's proprietary industrial electrode recipe applying "Curved Graphene" as active material in a planetary mixer (Fig. 6a). Following, the resulting slurry (solid content of 30–35 wt%) was double-side coated on a pilot line (Fig. 6b, line speed below 2 m min^{-1}, 5 m of drying oven) and calendered in Skeleton's industrial calendar (Fig. 6c) to decrease the resistance in terms of ESR and to increase the electrode density (>20% compression rate), consequently, increasing the overall amount of carbon inside the cell. After slitting the material to the desired electrode width (125 mm total width) (Fig. 6d), two electrode and separator rolls were joined and wound to an electrode/separator assembly (jelly-roll, Fig. 6e–f). Finally, the current collector tabs were laser welded to the positive and negative terminal (uncoated area), and the resulting jelly-roll-to-tab configuration was transferred into the can. After drying the cell at an elevated temperature of >120 °C under vacuum (<10 mbar) for >12 h, cells were filled under an inert atmosphere with a commercially available electrolyte and, finally, closed with an aluminum pin. The final cell is shown in Fig. 6g and a comparable commercially available application in the same industrial cell format is showcased in Fig. 6f.

Skeleton's standard SCA3200 cell format has to pass the same production steps. The only difference between standard production and the demonstrator is the used active material, namely "Curved Graphene", which increases the overall capacitance of the cell to >5000 F within the same cell format.

3.5. Demonstrator testing

The finally assembled industrial demonstrator consists of "Curved Graphene"-based electrodes, and a high molarity pyrrolidinium-based electrolyte, and was characterized by commonly used electrochemical test procedures for EDLCs, namely constant current, constant voltage or float, constant power, and self-discharge test. The constant current measurement depicted in Fig. 7a shows the high rate capability of the demonstrator, showcasing the ability to still provide high power with increased energy density. In a current range between 50 and 300 A, the capacitance of the device remains stable around 5000 F. However, the amount of stored charges slightly decreases from 7578 C to 7110 C due to the cell resistance, which causes an increasing ohmic drop with increasing current. This phenomenon underlines the important role of cell resistance when handling these high currents since it directly reduces the amount of energy that can be stored at increasing current rates. The Ragone plot shown in Fig. 7b highlights the high-power capability of the demonstrator indicating only minor losses in specific energy with increasing power.

Nowadays, supercapacitors are applied in a variety of different applications which are requiring different energy release/uptake. Since EDLCs store charges physically on the electrode surface, the self-discharge of this type of system is naturally relatively high compared to other energy storage technologies. This self-discharge can be characterized by applying a constant voltage to the cell and analyzing the current required to keep the cell at the defined voltage. Fig. 7c shows the current, the so-called leakage current, required to maintain the charged state at different voltages. It is visible that the self-discharging current decreases fast after reaching the voltage limit which can be attributed to the rearrangement of charges inside the electrical double-layer [47]. After holding the voltage constant for about 3 h, the self-discharge becomes diffusion controlled and the current decreases slightly until reaching a nearly constant value. Additionally, no major differences in the behavior of the leakage current between the different voltage limits can be observed. This highlights the stability of the electrolyte under the test conditions since the decomposition of the cell components by parasitic reactions would consume electrons, and, thus would lead to an increase in the base current [45].

In order to investigate the stability of the materials in an industrial cell format within a comparable industrial environment, a floating test at 65 °C in a time frame of 1500 h with a constant voltage of 2.85 V was performed. The result is shown in Fig. 8. The demonstrator cell features a capacitance retention of 78% after 1368 h of floating (Fig. 8a). During

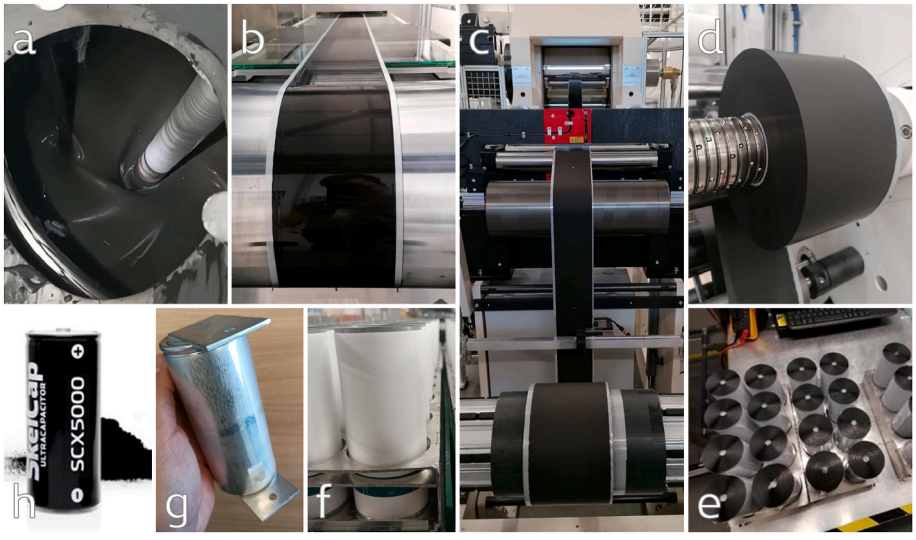

Fig. 6. Fabrication of CDC-based electrodes and industrial cell format demonstrator: a) Slurry mixing, b) coating, c) calendaring, d) slitting, e-f) jelly-rolls before cell assembly, g) final demonstrator cell with the dimensions Ø = 60 mm and height = 138 mm, and h) final industrial application in the same cell format.

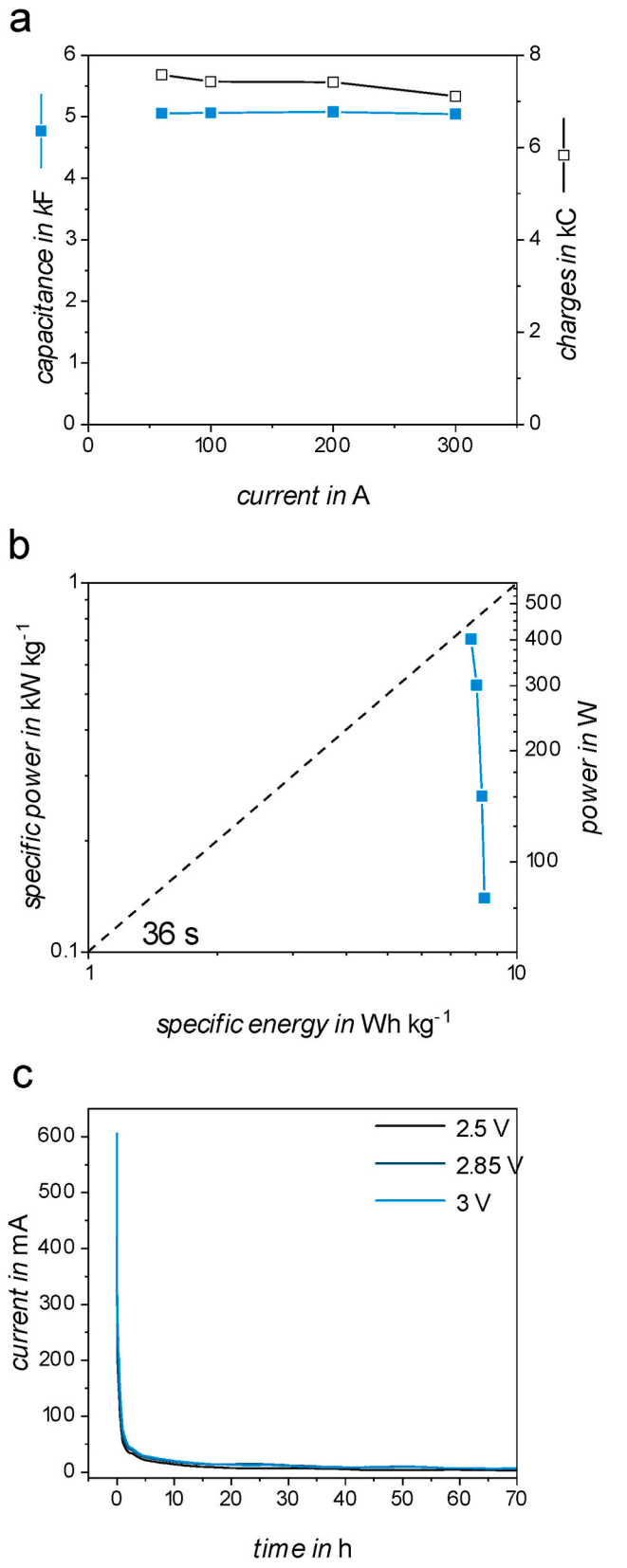

Fig. 7. a) Profile of capacitance and stored charges during constant current measurement at different currents of the demonstrator, b) Ragone plot of the demonstrator obtained by constant power measurement, and c) Comparison of the current profiles of the demonstrator at different constant voltages.

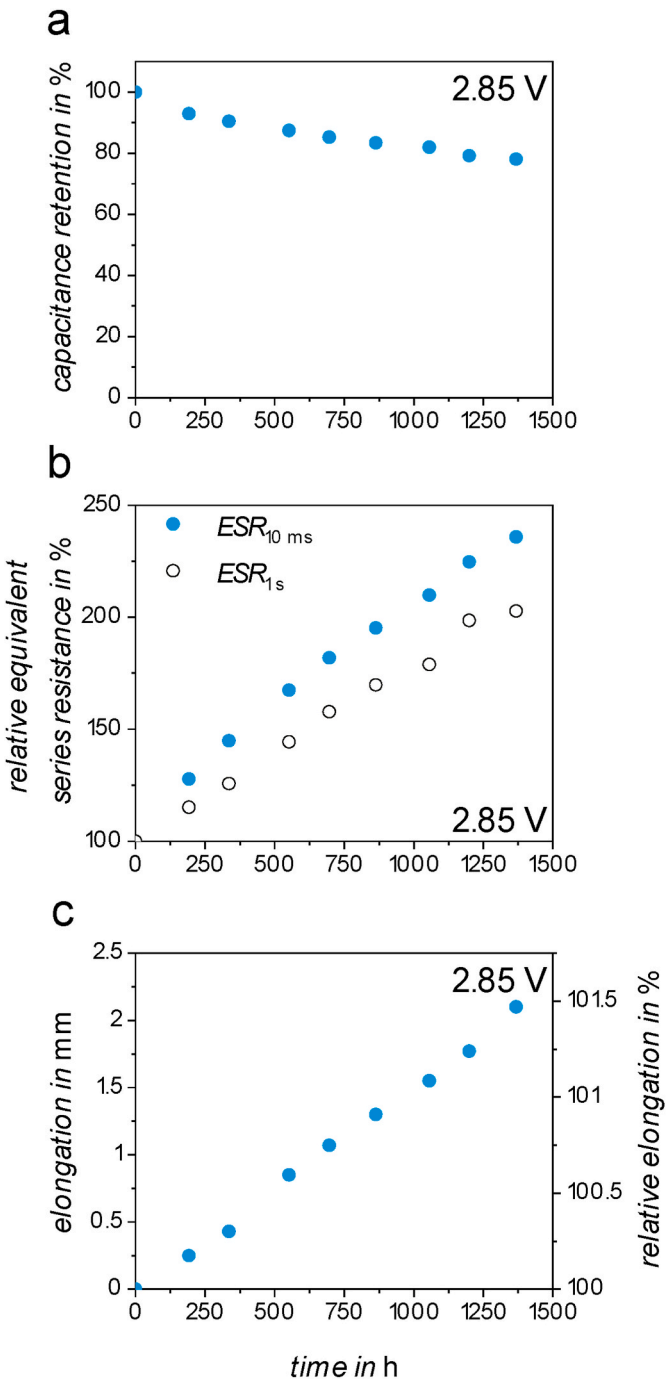

Fig. 8. Profile of a) capacitance retention, b) relative equivalent series resistance, and c) elongation and relative elongation of the industrial demonstrator cell during floating at 2.85 V for nearly 1500 h.

the complete floating test, the equivalent series resistance (Fig. 8b) increases to 236% when evaluated after 10 ms and by 202% when calculated after 1 s. Since floating tests at the maximum operative voltage are extremely demanding for the device, these tests lead to strong cell degradation. The elongation of the whole EDLC can also be a severe issue for the final application. During 1368 h of the floating test, the cell elongates by 2.1 mm which equals a relative increase of roughly 1.5% (Fig. 8c). This is caused by the evolution of gaseous decomposition products that occur during the aging of the device. Based on the utilized materials, different degradation products can be formed. While the electrolyte can dissolve various decomposition products, the formation of gases in the electrode-electrolyte interphase can lead to pore blocking

and an overall increase in the internal pressure of the cell resulting in the elongation of the cell body [48]. Considering the mechanical properties of the cell design, >2 mm of elongation is already the maximum the cell can elongate during aging due to gas evolution. Afterward, the cell classically vents via the safety valve.

The demonstration of "Curved Graphene" as active material in combination with other new materials (binder, electrolyte) in a large standard industrial cylindrical supercapacitor cell format shows promising results in terms of energy, power, and lifetime. These results are the first step for the commercialization of this new class of active material in Skeleton's supercapacitors. Considering that the production process was not optimized in terms of slurry recipe, welding steps, and electrode balancing – all highly relevant impactors on cell performance and lifetime behavior – the results are highly promising and showcase the potential for next-generation EDLC technology. Given that "Curved Graphene" was supplied out of industrial pilot reactors, it is reasonable to assume further improvements during the industrialization and scale-up processes, reaching an even higher purity of the material and minimizing side reactions and gas evolution during aging.

4. Conclusion

Transferring academic research to industrial applications is of high importance in order to solve the problems of our modern society. In this manuscript, we describe the realization of an industrial format EDLC demonstrator based on novel materials and their electrochemical performance evaluation.

The application of "Curved Graphene" instead of standard activated carbons derived from biomass, such as coconut shells, offers superior pore size distribution, as well as a lower content of heteroatoms. Alternative and green binder formulations based on polysaccharides and CMC offer improved film flexibility as well as higher achievable electrode and energy densities than commonly used binders. The improved electrolyte is based on pyrrolidinium-based salts in ACN which show increased stability compared to the industrial state-of-the-art. The final demonstrator cell displayed a nominal capacitance of 5000 F with a specific energy and energy density of up to 8.4 Wh kg^{-1} and 12.2 Wh L^{-1}, respectively, as well as a remarkable lifetime with a capacitance retention of 77% after floating for 1400 h at 2.85 V and 65 °C. These impressive cell properties achieved by the combination of novel materials tested in a non-optimized industrial format demonstrator cell show the pathway to increase the performance of EDLCs substantially.

CRediT authorship contribution statement

Lukas Köps: carried out the experimental work reported in the manuscript and wrote the article, Writing – original draft. **Peter Ruschhaupt:** carried out the experimental work reported in the manuscript and wrote the article, Writing – original draft. **Chris Guhrenz:** carried out the experimental work reported in the manuscript and wrote the article, Writing – original draft. **Philipp Schlee:** wrote/finalized the article. **Sebastian Pohlmann:** wrote/finalized the article. **Alberto Varzi:** wrote/finalized the article. **Stefano Passerini:** wrote/finalized the article and. **Andrea Balducci:** wrote/finalized the article.

Declaration of competing interest

The authors declare that they have no known competing financial interests or personal relationships that could have appeared to influence the work reported in this paper.

Data availability

Data will be made available on request.

Acknowledgments

The authors would like to thank the Bundesministerium für Wirtschaft und Energie (BMWi) within the project "ULTIMATE" (03ET6131) for the financial support. We thank Andrew Burke (UC Davis) for the electrochemical characterization of the industrial supercapacitor cell prototype and Peter Schiffels and Karsten Thiel (Fraunhofer IFAM) for the provision of SEM and TEM images of Curved Graphene.

This demonstrator has been realized utilizing the most interesting materials developed within the collaborative project "ULTIMATE – Ultracapacitors based on innovative materials for increased energy storage capability", funded by the Bundesministerium für Wirtschaft und Energie (BMWi) of Germany.

Appendix A. Supplementary data

Supplementary data to this article can be found online at https://doi.org/10.1016/j.jpowsour.2023.233016.

References

[1] J. Kalhoff, G.G. Eshetu, D. Bresser, S. Passerini, Safer electrolytes for lithium-ion batteries: state of the art and perspectives, ChemSusChem 8 (2015) 2154–2175, https://doi.org/10.1002/cssc.201500284.
[2] Z. Lin, E. Goikolea, A. Balducci, K. Naoi, P.L. Taberna, M. Salanne, G. Yushin, P. Simon, Materials for supercapacitors: when Li-ion battery power is not enough, Mater, Today Off. 21 (2018) 419–436, https://doi.org/10.1016/j.mattod.2018.01.035.
[3] P. Simon, Y. Gogotsi, B. Dunn, Materials science. Where do batteries end and supercapacitors begin? Science 343 (2014) 1210–1211, https://doi.org/10.1126/science.1249625.
[4] F. Beguin, V. Presser, A. Balducci, E. Frackowiak, Carbons and electrolytes for advanced supercapacitors, Adv. Mater. 26 (2014) 2219–2251, https://doi.org/10.1002/adma.201304137.
[5] P. Simon, Y. Gogotsi, Capacitive energy storage in nanostructured carbon-electrolyte systems, Acc. Chem. Res. 46 (2013) 1094–1103, https://doi.org/10.1021/ar200306b.
[6] B. Babu, P. Simon, A. Balducci, Fast charging materials for high power applications, Adv. Energy Mater. 10 (2020), 2001128, https://doi.org/10.1002/aenm.202001128.
[7] S. Pohlmann, C. Ramirez-Castro, A. Balducci, The influence of conductive salt ion selection on EDLC electrolyte characteristics and carbon-electrolyte interaction, J. Electrochem. Soc. 162 (2015) A5020–A5030, https://doi.org/10.1149/2.0041505jes.
[8] L.H. Hess, L. Wittscher, A. Balducci, The impact of carbonate solvents on the self-discharge, thermal stability and performance retention of high voltage electrochemical double layer capacitors, Phys. Chem. Chem. Phys. 21 (2019) 9089–9097, https://doi.org/10.1039/c9cp00483a.
[9] S.X. Hu, S.L. Zhang, N. Pan, Y.L. Hsieh, High energy density supercapacitors from lignin derived submicron activated carbon fibers in aqueous electrolytes, J. Power Sources 270 (2014) 106–112, https://doi.org/10.1016/j.jpowsour.2014.07.063.
[10] L. Köps, P. Zaccagnini, C.F. Pirri, A. Balducci, Determination of reliable resistance values for electrical double-layer capacitors, J. Power Sources Adv. 16 (2022), 100098, https://doi.org/10.1016/j.powera.2022.100098.
[11] A. Varzi, C. Schutter, J. Krummacher, R. Raccichini, C. Wolff, G.T. Kim, S. Rosler, B. Blumenroder, T. Schubert, S. Passerini, A. Balducci, A 4 Farad high energy electrochemical double layer capacitor prototype operating at 3.2 V (IES prototype), J. Power Sources 326 (2016) 162–169, https://doi.org/10.1016/j.jpowsour.2016.06.123.
[12] C. Schütter, S. Pohlmann, A. Balducci, Industrial requirements of materials for electrical double layer capacitors: impact on current and future applications, Adv. Energy Mater. 9 (2019), 1900334, https://doi.org/10.1002/aenm.201900334.
[13] T.P. Sumangala, M.S. Sreekanth, A. Rahaman, Applications of supercapacitors, in: K.K. Kar (Ed.), Handbook of Nanocomposite Supercapacitor Materials III, Springer International Publishing, 2021, pp. 367–393.
[14] D. Lasrado, S. Ahankari, K.K. Kar, Global trends in supercapacitors, in: K.K. Kar (Ed.), Handbook of Nanocomposite Supercapacitor Materials III, Springer International Publishing, 2021, pp. 329–365.
[15] S.L. Zhang, N. Pan, Supercapacitors performance evaluation, Adv. Energy Mater. 5 (2015), 1401401, https://doi.org/10.1002/aenm.201401401.
[16] J.Y. Zhao, A.F. Burke, Review on supercapacitors: technologies and performance evaluation, J. Energy Chem. 59 (2021) 276–291, https://doi.org/10.1016/j.jechem.2020.11.013.
[17] R. Vicentini, J.P. Aguiar, R. Beraldo, R. Venâncio, F. Rufino, L.M. Da Silva, H. Zanin, Ragone plots for electrochemical double-layer capacitors, Batter. Supercaps 4 (2021) 1291–1303, https://doi.org/10.1002/batt.202100093.
[18] L.H. Hess, A. Balducci, 1,2-butylene carbonate as solvent for EDLCs, Electrochim. Acta 281 (2018) 437–444, https://doi.org/10.1016/j.electacta.2018.05.168.

[19] P. Ruschhaupt, A. Varzi, S. Passerini, Natural polymers as green binders for high-loading supercapacitor electrodes, ChemSusChem 13 (2020) 763–770, https://doi.org/10.1002/cssc.201902863.
[20] M.D. Stoller, R.S. Ruoff, Best practice methods for determining an electrode material's performance for ultracapacitors, Energy Environ. Sci. 3 (2010) 1294–1301, https://doi.org/10.1039/c0ee00074d.
[21] L. Köps, F.A. Kreth, A. Bothe, A. Balducci, High voltage electrochemical capacitors operating at elevated temperature based on 1,1-dimethylpyrrolidinium tetrafluoroborate, Energy Storage Mater. 44 (2022) 66–72, https://doi.org/10.1016/j.ensm.2021.10.006.
[22] A. Balducci, Electrolytes for high voltage electrochemical double layer capacitors: a perspective article, J. Power Sources 326 (2016) 534–540, https://doi.org/10.1016/j.jpowsour.2016.05.029.
[23] A. Brandt, S. Pohlmann, A. Varzi, A. Balducci, S. Passerini, Ionic liquids in supercapacitors, MRS Bull. 38 (2013) 554–559, https://doi.org/10.1557/mrs.2013.151.
[24] A. Krause, A. Balducci, High voltage electrochemical double layer capacitor containing mixtures of ionic liquids and organic carbonate as electrolytes, Electrochem. Commun. 13 (2011) 814–817, https://doi.org/10.1016/j.elecom.2011.05.010.
[25] Z.N. Li, S. Gadipelli, Y.C. Yang, G.J. He, J. Guo, J.T. Li, Y. Lu, C.A. Howard, D.J. L. Brett, I.P. Parkin, F. Li, Z.X. Guo, Exceptional supercapacitor performance from optimized oxidation of graphene-oxide, Energy Storage Mater. 17 (2019) 12–21, https://doi.org/10.1016/j.ensm.2018.12.006.
[26] H. Park, J. Chung, H. Yong, J. Jung, C. Jung, Roles of gel polymer electrolytes for high-power activated carbon supercapacitors: ion reservoir and binder-like effects, RSC Adv. 10 (2020) 4690–4697, https://doi.org/10.1039/c9ra08765f.
[27] P. Simon, Y. Gogotsi, Materials for electrochemical capacitors, Nat. Mater. 7 (2008) 845–854, https://doi.org/10.1038/nmat2297.
[28] A. Bothe, A. Balducci, The impact of the thermal stability of non-conventional electrolytes on the behavior of high voltage electrochemical capacitors operating at 60 °C, Electrochim. Acta 374 (2021), 137919, https://doi.org/10.1016/j.electacta.2021.137919.
[29] S. Pohlmann, Metrics and methods for moving from research to innovation in energy storage, Nat. Commun. 13 (2022), https://doi.org/10.1038/s41467-022-29257-w.
[30] L.H. Hess, A. Balducci, Glyoxal-based solvents for electrochemical energy-storage devices, ChemSusChem 11 (2018) 1919–1926, https://doi.org/10.1002/cssc.201800375.
[31] Skeleton Technologies, SkelCap Supercapacitor Data Sheet, 2021 acessed, https://1188159.fs1.hubspotusercontent-na1.net/hubfs/1188159/02-DS-211222-SKELCAP-SCA-1B.pdf. (Accessed 3 November 2022).
[32] M.K.B. Gratuito, T. Panyathanmaporn, R.A. Chumnanklang, N. Sirinuntawittaya, A. Dutta, Production of activated carbon from coconut shell: optimization using response surface methodology, Bioresour. Technol. 99 (2008) 4887–4895, https://doi.org/10.1016/j.biortech.2007.09.042.
[33] W.M.A.W. Daud, W.S.W. Ali, Comparison on pore development of activated carbon produced from palm shell and coconut shell, Bioresour. Technol. 93 (2004) 63–69, https://doi.org/10.1016/j.biortech.2003.09.015.
[34] C.-L. Yeh, H.-C. Hsi, K.-C. Li, C.-H. Hou, Improved performance in capacitive deionization of activated carbon electrodes with a tunable mesopore and micropore ratio, Desalination 367 (2015) 60–68, https://doi.org/10.1016/j.desal.2015.03.035.
[35] F. Stoeckli, T.A. Centeno, On the characterization of microporous carbons by immersion calorimetry alone, Carbon 35 (1997) 1097–1100, https://doi.org/10.1016/s0008-6223(97)00067-5.
[36] F. Stoeckli, T.A. Centeno, On the determination of surface areas in activated carbons, Carbon 43 (2005) 1184–1190, https://doi.org/10.1016/j.carbon.2004.12.010.
[37] T.A. Centeno, F. Stoeckli, The assessment of surface areas in porous carbons by two model-independent techniques, the DR equation and DFT, Carbon 48 (2010) 2478–2486, https://doi.org/10.1016/j.carbon.2010.03.020.
[38] A.F. Burke, J. Zhao, Past, present and future of electrochemical capacitors: technologies, performance and applications, J. Energy Storage 35 (2021), 102310, https://doi.org/10.1016/j.est.2021.102310.
[39] P. Kurzweil, J. Schottenbauer, C. Schell, Past, present and future of electrochemical capacitors: pseudocapacitance, aging mechanisms and service life estimation, J. Energy Storage 35 (2021), 102311, https://doi.org/10.1016/j.est.2021.102311.
[40] A. Varzi, S. Passerini, Enabling high areal capacitance in electrochemical double layer capacitors by means of the environmentally friendly starch binder, J. Power Sources 300 (2015) 216–222, https://doi.org/10.1016/j.jpowsour.2015.09.065.
[41] B.A. Mei, O. Munteshari, J. Lau, B. Dunn, L. Pilon, Physical interpretations of nyquist plots for EDLC electrodes and devices, J. Phys. Chem. C 122 (2018) 194–206, https://doi.org/10.1021/acs.jpcc.7b10582.
[42] M. Ender, A. Weber, I.-T. Ellen, Analysis of three-electrode setups for AC-impedance measurements on lithium-ion cells by FEM simulations, J. Electrochem. Soc. 159 (2011) A128–A136, https://doi.org/10.1149/2.100202jes.
[43] L.W. Le Fevre, R. Fields, E. Redondo, R. Todd, A.J. Forsyth, R.A.W. Dryfe, Cell optimisation of supercapacitors using a quasi-reference electrode and potentiostatic analysis, J. Power Sources 424 (2019) 52–60, https://doi.org/10.1016/j.jpowsour.2019.03.062.
[44] D. Weingarth, A. Foelske-Schmitz, A. Wokaun, R. Kotz, PTFE bound activated carbon-A quasi-reference electrode for ionic liquids, Electrochem. Commun. 18 (2012) 116–118, https://doi.org/10.1016/j.elecom.2012.02.040.
[45] P. Ruschhaupt, S. Pohlmann, A. Varzi, S. Passerini, Determining realistic electrochemical stability windows of electrolytes for electrical double-layer capacitors, Batter. Supercaps 3 (2020) 698–707, https://doi.org/10.1002/batt.202000009.
[46] J. Krummacher, A. Balducci, Al(TFSI)3 as a conducting salt for high-voltage electrochemical double-layer capacitors, Chem. Mater. 30 (2018) 4857–4863, https://doi.org/10.1021/acs.chemmater.8b02253.
[47] L.H. Hess, N. Fulik, J. Röhner, E. Zhang, S. Kaskel, E. Brunner, A. Balducci, The role of diffusion processes in the self-discharge of electrochemical capacitors, Energy Storage Mater. 37 (2021) 501–508, https://doi.org/10.1016/j.ensm.2021.02.007.
[48] F.A. Kreth, L.H. Hess, A. Balducci, In-operando GC-MS: a new tool for the understanding of degradation processes occurring in electrochemical capacitors, Energy Storage Mater. 56 (2023) 192–204, https://doi.org/10.1016/j.ensm.2023.01.014.